

## Citric Acid Adsorption on TiO<sub>2</sub> Nanoparticles in Aqueous Suspensions at Acidic and Circumneutral pH: Surface Coverage, Surface Speciation, and Its Impact on Nanoparticle–Nanoparticle Interactions

Imali A. Mudunkotuwa and Vicki H. Grassian\*

*Department of Chemistry, University of Iowa, Iowa City, Iowa 52246*

Received July 16, 2010; E-mail: vicki-grassian@uiowa.edu

**Abstract:** Citric acid plays an important role as a stabilizer in several nanomaterial syntheses and is a common organic acid found in nature. Here, the adsorption of citric acid onto TiO<sub>2</sub> anatase nanoparticles with a particle diameter of ca. 4 nm is investigated at circumneutral and acidic pHs. This study focuses on both the details of the surface chemistry of citric acid on TiO<sub>2</sub>, including measurements of surface coverage and speciation, and its impact on nanoparticle behavior. Using macroscopic and molecular-based probes, citric acid adsorption and nanoparticle interactions are measured with quantitative solution phase adsorption measurements, attenuated total reflection-FTIR spectroscopy, dynamic light scattering techniques, and zeta-potential measurements as a function of solution pH. The results show that surface coverage is a function of pH and decreases with increasing pH. Surface speciation differs from the bulk solution and is time dependent. After equilibration, the fully deprotonated citrate ion is present on the surface regardless of the highly acidic solution pH indicating pK<sub>a</sub> values of surface adsorbed species are lower than those in solution. Nanoparticle interactions are also probed through measurements of aggregation and the data show that these interactions are complex and depend on the detailed interplay between bulk solution pH and surface chemistry.

### Introduction

Citric acid is a tricarboxylic acid, with pK<sub>a1</sub> = 3.13, pK<sub>a2</sub> = 4.76, pK<sub>a3</sub> = 6.40, that can form several species (H<sub>3</sub>Cit, H<sub>2</sub>Cit<sup>-</sup>, HCit<sup>2-</sup>, and Cit<sup>3-</sup>) depending on solution pH (see Figure 1 and Table 1). In addition to its natural abundance in the environment, citrate ion is often used in nanomaterials synthesis to control both the size and morphology of nanomaterials.<sup>1–3</sup> Because the citrate ion is a useful capping group that can undergo facile exchange with other functional groups, it is an important surface ligand for the preparation of a wide range of nanomaterials with complex surface functionality that can be used in a number of biomedical and sensor applications.<sup>1–4</sup> Furthermore, Yin et al. and Liu et al. report selective formation of anatase nanocrystallites from TiCl<sub>4</sub> in hydrothermal autoclaving in the presence of organic acids including citric acid.<sup>5,6</sup> These studies show that phase composition and size control are sensitive to the organic acid used due to surface adsorption during crystal growth.

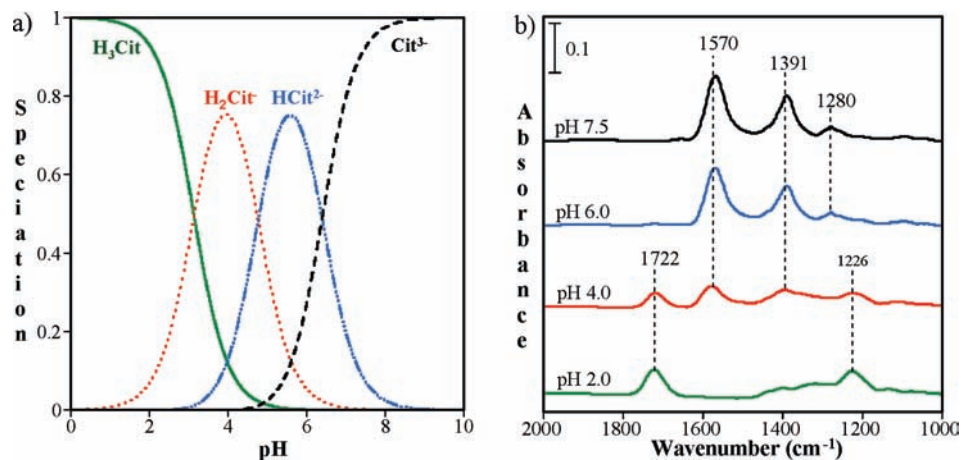
Citric acid is also found in human plasma (0.1 mM) that can result in its interaction with foreign species entering the body.<sup>7</sup>

Additionally, the estimated total organic acid concentration in soil solutions has been reported to be in the range of 10–100 μM and can reach as high as 1 mM in the rhizosphere.<sup>8</sup> These organic acids are being heavily studied as a result of their role in mineral dissolution, detoxification of metals as chelating agents, and ultimately determining the fate and transformation of inorganic pollutants.<sup>9–11</sup> Citric acid based studies are also considered to be good analogues for the functional groups in more complex humic acids that can provide insight into adsorption mechanisms.

The focus of this study is on surface adsorption and surface chemistry of citric acid on ca. 4 nm TiO<sub>2</sub> (anatase) at circumneutral and acidic pH as nanoparticle surfaces play a key role in their behavior. Although our particular interests are related to the chemistry of nanomaterials in the environment, the results of this study can be more broadly applied to understanding the detailed surface chemistry of this important ligand. In particular, the adsorption of citric acid has been studied here with emphasis on pH effects using quantitative solution phase adsorption measurements to determine surface coverage and ATR-FTIR spectroscopy to probe surface speciation. Additionally, nanoparticle–nanoparticle interactions and the stability of nanoparticle suspensions with and without citric

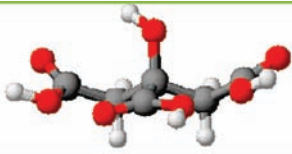
- (1) Ojea-Jimenez, I.; Puentes, V. *J. Am. Chem. Soc.* **2009**, *132*, 5322.
- (2) Xue, C.; Metraux, G. S.; Millstone, J. E.; Mirkin, C. A. *J. Am. Chem. Soc.* **2008**, *130*, 8337.
- (3) Ji, X. H.; Song, X. N.; Li, J.; Bai, Y. B.; Yang, W. S.; Peng, X. G. *J. Am. Chem. Soc.* **2007**, *129*, 13939.
- (4) Ozkar, S.; Finke, R. G. *J. Am. Chem. Soc.* **2002**, *124*, 5796.
- (5) Yin, H. B.; Wada, Y.; Kitamura, T.; Sumida, T.; Hasegawa, Y.; Yanagida, S. *J. Mater. Chem.* **2002**, *12*, 378.
- (6) Liu, Y.; Liu, C. Y.; Zhang, Z. Y. *Chem. Eng. J.* **2008**, *138*, 596.
- (7) Dakanali, M.; Raptopoulou, C. P.; Terzis, A.; Lakatos, A.; Banyai, I.; Kiss, T.; Salifogiou, A. *Inorg. Chem.* **2003**, *42*, 252.

- (8) Huang, P. M.; Wang, M. K.; Chiu, C. Y. *Pedobiologia* **2005**, *49*, 609.
- (9) Kubicki, J. D.; Schroeter, L. M.; Itoh, M. J.; Nguyen, B. N.; Apitz, S. E. *Geochim. Cosmochim. Acta* **1999**, *63*, 2709.
- (10) Lackovic, K.; Johnson, B. B.; Angove, M. J.; Wells, J. D. *J. Colloid Interface Sci.* **2003**, *267*, 49.
- (11) Lindgren, M.; Loring, J. S.; Persson, P. *Langmuir* **2009**, *25*, 10639.



**Figure 1.** (a) Calculated speciation of citric acid, a tricarboxylic acid, from  $pK_a$  values as a function of pH. (b) ATR-FTIR spectra of 100 mM citric acid solutions at different pH: 2.0, 4.0, 6.0, and 7.5.

**Table 1.**  $pK_a$  Values at 298 K for Citric Acid (H<sub>3</sub>Cit)

	$pK_a$
$H_3Cit \rightleftharpoons H^+ + H_2Cit^-$	3.13
$H_2Cit^- \rightleftharpoons H^+ + HCit^{2-}$	4.76
$HCit^{2-} \rightleftharpoons H^+ + Cit^{3-}$	6.40

acid have been followed with light scattering techniques as a function of pH.

Although few studies integrate these different types of measurements to provide a quantitative description of surface coverage, surface speciation, and nanoparticle interactions, there is the potential to gain additional insights into the adsorption of citrate on nanoparticle surfaces by integrating these experimental results. Thus, the current study provides important insights into the use of citrate as a capping agent and stabilizer of nanoparticles in aqueous suspensions. It also provides much needed experimental data on the interactions of nanomaterials with common ligands found in the environment.

## Experimental Section

**Nanoparticle Characterization.** Powder X-ray diffraction (XRD) was used to determine the bulk crystalline phase of TiO<sub>2</sub> nanoparticles. Diffraction patterns were collected using a Rigaku Miniflex II diffractometer with a Co source. The specific surface area of the particles was determined from seven-point N<sub>2</sub>-BET adsorption isotherm measurements using a Quantachrome 4200e surface area analyzer. Samples were degassed for 3 h at 573 K prior to the analysis.

**Quantitative Solution Phase Adsorption/Desorption Studies.** Adsorption and desorption studies were conducted at pH 2.0, 4.0, 6.0, and 7.5. Stock solutions of 100 mM citric acid were prepared at pH 2.0, 4.0, 6.0, and 7.5 at 293 K. Solutions at pH 2.0 and 4.0 contained 0.01 and 0.0001 N HCl solutions, while solutions at pH

6.0 and 7.5 contained 25 mM of MES and HEPES, respectively. pH adjustment at higher pHs was done by NaOH solution (8 M). As a result of the ionic strength of pH 2.0 solution and pH adjustments, all the solutions were prepared to have an ionic strength of 0.03 M NaCl. The adsorption experiments were conducted according to the following protocol.

From the solutions prepared above, 6 mL aliquots were added into 7 mL glass vials. To each of these vials, appropriate volumes of citric acid (100 mM) were added to obtain a concentration range of 0.1–5 mM in the reactors. Prior to the addition of the solid, 1 mL of sample was drawn out from each vial for the quantification of the initial citric acid concentration. A TiO<sub>2</sub> solid loading of 2.0 g/L in the reactors was used. After mixing, the reactors were crimp sealed, covered in aluminum foil to inhibit any photo-induced chemistry, and mixed on a Cole-Parmer circular rotator for 24 h. After completion of the mixing, suspension pH was measured. Then, from each reactor two aliquots (~1 mL each) were drawn out with a disposable syringe, passed through a 0.2  $\mu$ m syringe-driven filter (Xperts) into separate centrifugation vials, and centrifuged at 14 000 rpm for 20 min to separate the solution from the TiO<sub>2</sub> nanoparticles.

One set of these samples was analyzed using an Agilent HPLC equipped with a diode array UV-vis detector at 226 nm using 0.01 N H<sub>2</sub>SO<sub>4</sub> as the mobile phase. The instrument response was measured with respect to known standards of citric acid and converted into aqueous phase concentrations. The standards were prepared fresh for each set of reactors. The concentration of the adsorbed citric acid was then determined using the difference of the initial and final citric acid concentrations in the aqueous phase.

Experiments were conducted to investigate the reversibility of citric acid adsorption onto TiO<sub>2</sub> nanoparticles. For an adsorption study conducted with 3 mM of citric acid, the suspension was divided into five 1 mL aliquots and centrifuged for 20 min. The supernatant was decanted off and the remaining particles were resuspended in fresh solutions of the same initial pH and transferred to a 7 mL glass vial, and the same procedure as in the adsorption study carried out to obtain the amount of citric acid in the solution.

### Quantitative Solution Phase Nanoparticle Dissolution Studies.

A second set of the samples discussed above for quantitative adsorption measurements were analyzed using a Varian Inductively Coupled Plasma Optical Emission Spectrophotometer (ICP-OES) for any dissolved titanium. These centrifuged samples were diluted to 5 mL with 1 M HCl solutions prior to analysis.

**ATR-FTIR Spectroscopy.** Solution phase attenuated total reflectance Fourier transform infrared (ATR-FTIR) spectroscopy measurements were recorded of 100 mM citric acid solutions prepared at several different pH values (pH 2.0, 4.0, 6.0, and 7.5) using a Thermo-Nicolet FTIR Spectrometer equipped with a

MCT/A detector. Additionally, citric acid adsorption onto TiO<sub>2</sub> surface was also probed with ATR-FTIR spectroscopy. For surface adsorption studies, a thin, evenly coated TiO<sub>2</sub> film was deposited onto an AMTIR crystal element in a horizontal ATR cell (Pike Technologies, Inc.). The film was prepared by placing a suspension of TiO<sub>2</sub> (1.5 mg in 1 mL of Optima water) onto the crystal and drying overnight. The deposited film was slowly flushed with a stream of water to eliminate any loosely bound particles. Citric acid solutions (0.1, 0.2, 0.5, 1, 2, 5, and 10 mM) of constant ionic strength were prepared and then introduced into the horizontal cell. Initially, spectra were collected after 5 min. Additional experiments were conducted at pH 2.0 and pH 6.0 for longer periods of time to equilibrate the solution. Spectra were collected in the spectral range extending from 500 to 4000 cm<sup>-1</sup> at an instrument resolution of 4 cm<sup>-1</sup>.

**Nanoparticle–Nanoparticle Interactions and Aggregation Measurements.** Nanoparticle–nanoparticle interactions and the aggregation behavior of 4 nm TiO<sub>2</sub> particle suspensions at 0.03–0.04 M ionic strength were examined at pH 2.0, 4.0, 6.0, and 7.5. Sedimentation experiments were conducted with a UV–vis spectrometer by monitoring the changes in the light scattering when passed through TiO<sub>2</sub> suspensions (2.0 g/L) as a function of time. Suspensions were prepared in a 1 cm path length cuvette, agitated, and placed in the UV–vis instrument and the amount of transmitted light ( $\lambda = 508$  nm) was measured over time. The solutions were left overnight to reach the steady state aggregation, and therefore, no aggregation was assumed to occur during the time of the measurement. Therefore, the sedimentation is solely attributed to the gravitational settling depending on the particle size. A linear relationship between the scattered light and the TiO<sub>2</sub> suspension concentrations was observed for particle suspension concentrations of 0.5–2.0 g/L at 508 nm (see Supplemental Figure 1).

A commercial dynamic light scattering (DLS) instrument (Malvern Zetasizer Nano ZS) equipped with a green laser at 532 nm was used to obtain the size distribution of aggregates in the absence and the presence of citric acid. For DLS measurements, suspensions were prepared at 0.01 g/L solid loading of TiO<sub>2</sub> in appropriate pH solutions. The pH solutions were passed through a 0.2  $\mu$ m syringe driven filter to minimize the influence of unwanted dust particles. Samples were allowed to sit overnight to ensure the aggregation had reached its steady state. Aggregate sizes were studied over a range of citric acid concentrations (0–0.2 mM).

In addition, the surface charge of the nanoparticles was measured using the zeta potential mode of the Malvern Zetasizer Nano ZS. All suspensions were prepared to have a solid loading of 0.05 g/L, 0.1 mM of citric acid, and a fixed ionic strength of 0.03 M. The suspensions were allowed to equilibrate for 24 h after mixing. Measurements were made at pH 2.0, 3.0, 4.0, 5.0, 6.0, and 7.0. These experiments were also conducted in the absence of citric acid.

**Reagents.** TiO<sub>2</sub> nanoparticles that were purchased from Nanostructured and Amorphous Materials, Inc. (Houston, TX). The vendor reported the nanoparticles to consist entirely of anatase with the primary particle size 5 nm.

Solution phase studies were conducted with 2-(*n*-morpholino)ethanesulfonic acid (MES; Sigma Aldrich;  $\geq 99\%$ ), 4-(2-hydroxyethyl)-1-piperazineethanesulfonic acid (HEPES; Sigma Aldrich,  $\geq 99.5\%$ ), or hydrochloric acid (HCl; Fisher Scientific; certified ACS plus). To adjust the pH, sodium hydroxide (NaOH; Fisher Scientific; certified ACS plus) was used. To keep the solution ionic speciation at a minimum, sodium chloride (NaCl; Fisher Scientific; certified ACS plus) was used to adjust ionic strength. The aqueous solutions of citric acid (Sigma Aldrich, 99.5% certified ACS plus) and all reactors were prepared using Optima water (Fisher Scientific).

## Results and Discussion

**Nanoparticle Characterization.** XRD analysis confirmed that the TiO<sub>2</sub> nanoparticles consist entirely of anatase. The measured surface area using a seven-point BET analysis showed an average value of  $219 \pm 3$  m<sup>2</sup>/g from four replicate measure-

**Table 2.** Quantitative Measurements of Saturation Surface Coverages for Citric Acid on TiO<sub>2</sub> Nanoparticles in Solution at pH 2.0, 4.0, 6.0, and 7.5

pH	surface coverage (molecules cm <sup>-2</sup> )
2.0	$9.7 \pm 0.4 \times 10^{13}$
4.0	$7.5 \pm 0.3 \times 10^{13}$
6.0	$6.3 \pm 0.5 \times 10^{13}$
7.5	$3.1 \pm 0.4 \times 10^{13}$

ments. A previous TEM characterization of these 5 nm particles has shown a size distribution between 2 and 5 nm with an average nanoparticle diameter of  $3.5 \pm 1.5$  nm.<sup>12</sup> These nanoparticles are referred to as 4 nm particles herein.

**Citric Acid Adsorption on TiO<sub>2</sub> Nanoparticles at  $T = 293$  K: Surface Coverage as  $f(\text{pH})$ .** Citric acid adsorption on 4 nm TiO<sub>2</sub> nanoparticles was carried out at pH 2.0, 4.0, 6.0, and 7.5. For 2 g/L of TiO<sub>2</sub> nanoparticles, the initial and the final pH of the reactors were the same for pH 2.0, 6.0, and 7.5, while the reactors with initial pH 4.0 was raised to values ranging from pH 4.5 to 5.5. The general trend of citric acid adsorption onto the TiO<sub>2</sub> nanoparticles is a decrease with increasing solution pH. The surface area normalized uptake of citric acid at saturation coverage is given in Table 2 and goes from  $9.7 \pm 0.4$  to  $3.1 \pm 0.4 \times 10^{13}$  molecules cm<sup>-2</sup> at the lowest and highest pH values of 2.0 and 7.5, respectively. Saturation coverage was determined to occur at concentrations greater than 2 mM (see Supplemental Figure 2) and these values represent the average of four different independent measurements of solution phase concentrations between 2 and 5 mM. The decrease in surface coverage by over a factor of 3 is not unexpected since the surface charge of TiO<sub>2</sub> nanoparticles and the citric acid species increase in negativity simultaneously with the increasing pH. Zeta potential measurements showed a zero point charge pH ( $\text{pH}_{\text{zpc}}$ ) of TiO<sub>2</sub> nanoparticles to be pH 4.2 in the absence of citric acid. This value is close to the  $\text{pH}_{\text{zpc}}$  (pH 4.6–6.5 for sizes between 3.6 and 8.1 nm) reported in the literature for TiO<sub>2</sub> nanoparticles of this size. Therefore, the surface charge of these particles is mostly positive for pH <4.0 and negative for pH >4.0.<sup>13</sup>

As shown in Figure 1a and Table 1, the major fraction of citrate species in the solution is neutral/monoanionic, mono/dianionic, and trianionic in these three pH ranges of <4.0, between 4.0 and 6.0, and >6.0, respectively. As the solution pH increases, the repulsive forces between the nanoparticles and the negatively charged anions increase resulting in the observed decrease in the uptake. This observed trend is in good agreement with previous studies on citric acid adsorption by goethite.<sup>10,11</sup> However, the degree of drop in citric acid uptake is smaller for the nanoscale TiO<sub>2</sub> particles compared to that of goethite in these studies with the 3-fold decrease when going from pH 5.5 to pH 8.0 for goethite in contrast to the 3-fold decrease from pH 2.0 to pH 7.5 for TiO<sub>2</sub> nanoparticles.

Reversibility measurements (90% particle recovery) showed that the adsorption of citric acid at all pH values was irreversible. Furthermore, the ATR-FTIR experiments showed no decrease in the peak intensities when the citrate adsorbed TiO<sub>2</sub> surface was washed with water which confirmed the results of the reversibility studies. Studies of citric acid adsorption onto iron and aluminum oxides have shown inner-sphere complexes

(12) Grassian, V. H.; O'Shaughnessy, P. T.; Adamcakova-Dodd, A.; Pettibone, J. M.; Thorne, P. S. *Environ. Health Perspect.* **2007**, *115*, 397.

(13) Guzman, K. A. D.; Finnegan, M. P.; Banfield, J. F. *Environ. Sci. Technol.* **2006**, *40*, 7688.

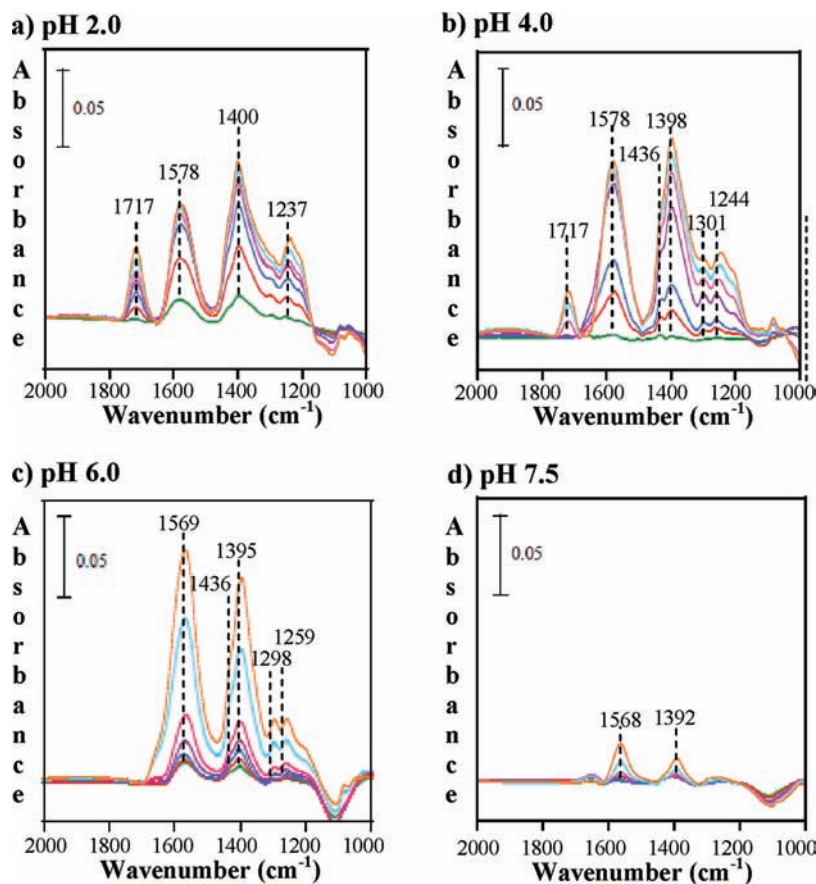


**Figure 2.** ATR-FTIR spectra of adsorbed citric acid as a function of initial concentration (0.1, 0.2, 0.5, 1, 2, 5, and 10 mM) at different pH: 2.0, 4.0, 6.0, and 7.5.

forming on the surface in the pH range considered.<sup>10,11,14</sup> Since inner-sphere surface complexation typically represents a more strongly coordinated surface species that can be irreversible at 293 K, it can be proposed that citric acid adsorption on TiO<sub>2</sub> nanoparticles is mostly likely inner sphere in nature (vide infra).

**Citric Acid Adsorption on TiO<sub>2</sub> Nanoparticles at  $T = 293$  K: Nanoparticle Dissolution as a  $f(\text{pH})$  with and without the Presence of Citric Acid.** Although from thermodynamics, bulk TiO<sub>2</sub> is known to be insoluble in aqueous media at 298 K, experimental observations have been made to suggest that for very small nanoparticles dissolution can occur given that solubility, due to size dependent surface free energies, is size dependent. Schmidt and Vogelsberger report that TiO<sub>2</sub> precipitated by the hydrolysis of titanium tetraisopropoxide shows saturation dissolution at micromoles per liter and that particle size, morphology, pH, and temperature were shown to affect dissolution behavior.<sup>15</sup> Because the current study is focused on 4 nm TiO<sub>2</sub>, measurements were done to determine if dissolution can occur for these nanoscale materials. Since citrate is potentially a polydentate adsorbate, it can form a strongly coordinating complex on the surface which can result in oxide dissolution associated with the simultaneous detachment of two metal cations from the surface.<sup>14,16</sup> However, ICP-OES studies showed no dissolution of TiO<sub>2</sub> nanoparticles taking place in the presence of citric acid under all pH conditions investigated.

**Citric Acid Adsorption on TiO<sub>2</sub> Nanoparticles at  $T = 293$  K: Solution Phase Speciation Compared to Surface Speciation as  $f(\text{pH})$ .** In solution, citric acid is fully protonated at pH 2.0, partially deprotonated at pH 4.0 and 6.0, and it is fully deprotonated at pH 7.5 (Figure 1a). As shown in Figure 1b, the fully deprotonated citrate ion has prominent absorption bands near 1570 and 1391 cm<sup>-1</sup> and a weak band around 1280 cm<sup>-1</sup>. The two prominent bands, 1570 and 1391 cm<sup>-1</sup>, are assigned to the asymmetric and symmetric stretching motions of the carboxylate group, respectively.<sup>9–11,14,17–20</sup> The weaker band at 1280 cm<sup>-1</sup> is assigned to coupled stretches and bends of the carboxylate group. With decreasing pH, the bands at 1570 and 1391 cm<sup>-1</sup> diminish in intensity and at pH 2.0 are no longer present. Instead, absorption bands at 1722 and 1226 cm<sup>-1</sup> are evident. These new bands correspond to the C=O stretching motion and coupled C–(OH) stretching and C–O–H bending motions, respectively.<sup>9–11,14,17–20</sup> ATR-FTIR solution phase spectra agree well with the calculated speciation fractions shown in Figure 1a.

Spectroscopic measurements as a  $f(\text{pH})$  gave useful information about the citrate-surface adsorbed complex. ATR-FTIR spectra of adsorbed citric acid onto TiO<sub>2</sub> nanoparticles as a function of citric acid concentrations (ranging from 0.1 to 10 mM) and pH are shown in Figure 2. These spectra were recorded

(14) Pirmin, C. H.; Thomas, J. G.; Ludwig, J. G. *J. Am. Ceram. Soc.* **1996**, *79*, 1857.

(15) Schmidt, J.; Vogelsberger, W. *J. Phys. Chem. B* **2006**, *110*, 3955.

(16) Johnson, S. B.; Brown, G. E.; Healy, T. W.; Scales, P. J. *Langmuir* **2005**, *21*, 6356.

(17) Hug, S. J.; Bahnmann, D. *J. Electron Spectrosc. Relat. Phenom.* **2006**, *150*, 208.

(18) Ojamae, L.; Aulin, C.; Pedersen, H.; Kall, P. O. *J. Colloid Interface Sci.* **2006**, *296*, 71.

(19) Max, J. J.; Chapados, C. *J. Phys. Chem. A* **2004**, *108*, 3324.

(20) Borer, P.; Hug, S. J.; Sulzberger, B.; Kraemer, S. M.; Kretzschmar, R. *J. Phys. Chem. C* **2007**, *111*, 10560.

**Table 3.** Vibrational Frequencies ( $\text{cm}^{-1}$ ) and Assignment of the Solution Phase and Initially Observed ( $t = 5$  min) Adsorbed Citric Acid Species on  $\text{TiO}_2$  Nanoparticles at pH 2.0, 4.0, 6.0, and 7.5<sup>a</sup>

mode of vibration	pH 2.0		pH 4.0		pH 6.0		pH 7.5	
	solution	surface $t = 5$ min	solution	surface $t = 5$ min	solution	surface $t = 5$ min	solution	surface $t = 5$ min
$\nu(\text{C}=\text{O})$	1722	1717	1720	1718	1721			
$\nu_{\text{as}}(\text{COO}^-)$		1579	1577	1578	1571	1569	1569	1569
$\nu_{\text{s}}(\text{COO}^-)$		1400	1395	1398	1391	1395	1391	1395
		1436*		1436*		1436*		1436*
$\nu(\text{C}-\text{OH})$					1094		1094	
$\nu(\text{OC}-\text{OH})+$	1226		1227	1244				
$\delta(\text{OC}-\text{OH})$								
$\delta(\text{CH}_2)$					1436		1436	
$\delta(\text{O}=\text{C}-\text{O}^-)$					1280	1298	1279	1292
						1259	1260	1262

<sup>a</sup> Asterisk (\*) denotes the shoulder arising due to the splitting of the symmetric stretch band of the carboxylate group for adsorbed citric acid.

5 min after introduction of the solution phase. A comparison of ATR-FTIR spectra recorded of 10 mM solution phase citric acid at all four pHs investigated to the spectra recorded in the presence of  $\text{TiO}_2$  (see Supplemental Figure 3) shows that there is no contribution of solution phase absorbance to the spectra shown in Figure 2.

These ATR-FTIR spectra shown in Figure 2 provide information on surface speciation and indicate differences from speciation in solution. The most prominent difference between the solution spectra (Figure 1b) and surface adsorbed spectra (Figure 2) is observed at pH 2.0. The bands at 1570 and 1391  $\text{cm}^{-1}$  which are not present in the pH 2.0 solution phase are present for adsorbed citric acid at pH 2.0. Furthermore, the band at 1722  $\text{cm}^{-1}$  observed clearly in the solution phase spectrum and in fact the most intense band in the spectrum is seen to shift to 1717  $\text{cm}^{-1}$  and is no longer the most intense band in the spectrum. The shift toward a lower value arises most likely as a result of the weakened  $\text{C}=\text{O}$  bond resulting from the interaction with the surface.

For other pH values, the spectra appear more similar between the solution phase and on the surface. However, upon closer inspection, it can be seen that the absorption bands for the surface adsorbed species are broad compared to solution phase. Furthermore, a shoulder peak at 1436  $\text{cm}^{-1}$  can be observed in all the spectra. In the literature (Table 3) for the solution phase spectra, the shoulder at 1436  $\text{cm}^{-1}$  is given as  $-\text{CH}_2-$  bending mode.<sup>21</sup> However, by inspecting Figure 2b which gives the surface adsorbed citric acid spectra at pH 4.0, it can clearly be seen that there is a distinct band appearing at 1436  $\text{cm}^{-1}$ . This band, as it grows, overlaps with the absorption at 1398  $\text{cm}^{-1}$ . These changes in spectral features suggest that the absorption bands in the surface spectra are a sum of several overlapping peaks. These observations support the proposed mode of citrate adsorption as an inner sphere complex, that is, inner sphere adsorptions are known to result in broader spectra and a higher splitting of several of the absorption bands.<sup>9</sup>

ATR-FTIR spectroscopy also reveals that the surface spectra are time dependent. Figure 3a shows this explicitly for pH 2.0. In these experiments, spectra were recorded as a function of time for up to 4 h. It can be seen from the spectra shown in Figure 3a that after 4 h the band at 1717  $\text{cm}^{-1}$  has disappeared from the spectrum and is no longer present. The intensity of this peak plotted as a function of time (Figure 3b) clearly demonstrates this. These data show that, at pH

2.0, the adsorbed species undergo deprotonation on the surface and yields the fully deprotonated citrate ion on the  $\text{TiO}_2$  nanoparticle surface (Figure 3c). These results suggest that there is an increase in the acidity of citric acid when adsorbed on the surface. In other words, the ability to deprotonate and the apparent  $\text{p}K_{\text{a}}$ 's of citric acid have decreased upon surface complexation and are below 2. However, it should be noted that at pH 4.0 and at a concentration of 10 mM similar ATR-FTIR data show that the  $\text{C}=\text{O}$  stretch peak does not decrease with time arising possibly due to differences in the mode of adsorption at different pH values, suggesting that the details of the nature of adsorption sites and coordination mode play a role in surface speciation.

It has been proposed that citrate adsorption on goethite results in the formation of inner-sphere complex with citrate coordination to the surface via at least one carboxylate group.<sup>9</sup> The spectra observed in the goethite study are similar to the spectra collected in this current study. With the observed deprotonation taking place on the surface, it can be proposed that the initial adsorption is via the carbonyl oxygen ( $\text{C}=\text{O}$ ), which result in the increased polarization of the  $\text{C}-\text{O}-\text{H}$  bonds leading to rapid loss of  $\text{H}^+$  (Figure 3c). At pH 2.0, all the carboxylic groups of the molecule appears to be bound to the surface as seen by the complete loss of the protonated  $\text{C}=\text{O}$  peak in the spectra collected as a function of time. But at pH 6.0, whether all the carboxylate groups are bound to the surface is less clear as deprotonation does not necessarily indicate surface coordination. However the increased breadth of the peaks are indicative of surface coordination as discussed above.

**Light Scattering and Zeta-Potential Measurements of  $\text{TiO}_2$  Nanoparticle Suspensions as a  $f(\text{pH})$  with and without the Presence of Citric Acid To Investigate Nanoparticle–Nanoparticle Interactions and Nanoparticle Aggregation.** The stability of the nanoparticle suspensions was investigated under the same conditions that the quantitative surface adsorption measurements were made. Sedimentation plots as a function of time are shown in Figure 4. These data show that nanoparticles settle out of solution as a function of time for nanoparticle concentrations of 2.0 g/L at pH 4.0, 6.0, and 7.5. Only at pH 2.0 are nanoparticle suspensions stable. Furthermore, the nanoparticle suspensions at pH 2.0 were visually stable for several days. This stabilization of  $\text{TiO}_2$  particle suspensions has been previously observed at highly acidic and basic conditions.<sup>22</sup> Complementary

(21) Pasilis, S. P.; Pemberton, J. E. *Geochim. Cosmochim. Acta* **2008**, *72*, 277.

(22) Martyanov, I. N.; Savinov, E. N.; Klabunde, K. J. *J. Colloid Interface Sci.* **2003**, *267*, 111.

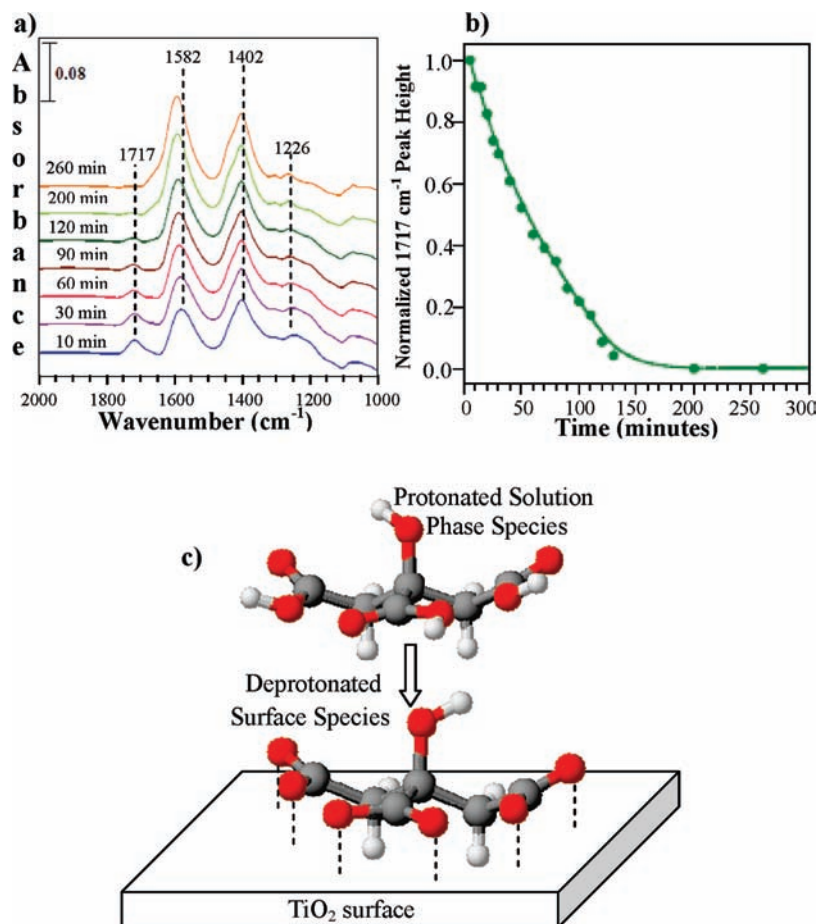


**Figure 3.** (a) ATR-FTIR spectra as a function of time show changes in surface speciation following adsorption of 10 mM adsorption at pH 2.0. (b) A plot of the normalized intensity of the  $\nu(\text{C}=\text{O})$  at  $1717\text{ cm}^{-1}$  as a function of time. (c) Cartoon representation of surface adsorption of citric acid from solution at pH 2.0.

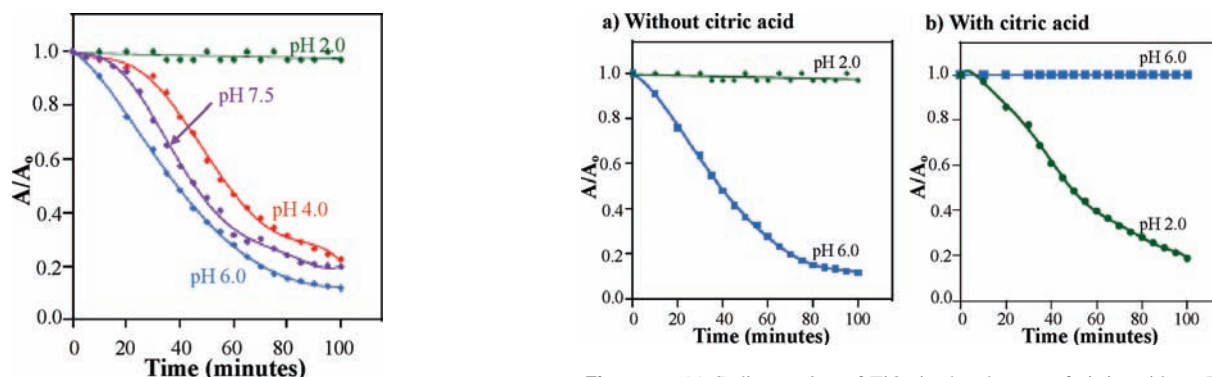


**Figure 4.** Sedimentation plots for TiO<sub>2</sub> in the absence of citric acid at different pH: 2.0, 4.0, 6.0, and 7.5.

DLS measurements gave the largest size distribution of aggregates at pH 6.0 and the smallest at pH 2.0 (vide infra).

According to Derjaguin, Landau, Verwey, and Overbeek theory (DLVO theory), the stability of a colloidal system is determined by the sum of van der Waals attractive forces and electrical double layer forces that exist between particles as they approach one another due to Brownian motion.<sup>14,16</sup> At pH 2.0, TiO<sub>2</sub> nanoparticles experience higher repulsive forces due to high surface protonation, hence, increased double layer formation. At pH 6.0 (which is in the range of  $\text{pH}_{\text{zpc}}$  for 4 nm TiO<sub>2</sub> nanoparticles), the surface charge is almost neutral and the double layer formation is almost zero. Therefore, the attractive

van der Waals forces as the pH increases begin to dominate resulting in increased aggregation.<sup>22</sup>

The aggregation behavior of the TiO<sub>2</sub> and nanoparticle–nanoparticle interactions alters in the presence of citric acid in highly acidic and circumneutral conditions. Sedimentation plots for pH 2.0 and pH 6.0 show that the presence of citric acid reverses the behavior seen in Figure 5. It is seen that citric acid causes a destabilization of solutions at pH 2.0 and significantly enhances the aggregation, whereas for pH 6.0, citric acid stabilizes nanoparticle suspensions. DLS measurements of nanoparticle suspensions at pH 2.0 and 6.0 as a function of increasing citric acid adsorption shown in Figure 6 complement

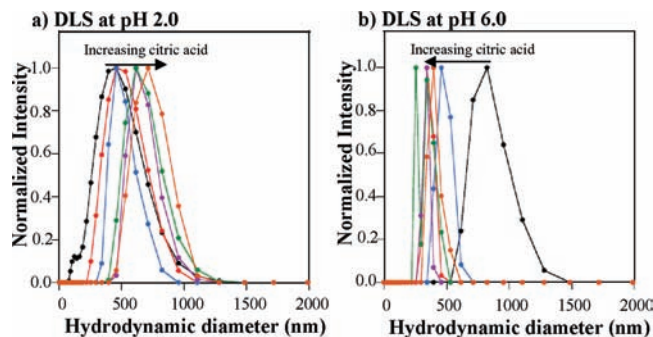


**Figure 6.** (a) Intensity normalized aggregate distribution for at pH 2.0. (b) Intensity normalized aggregate distribution at pH 6.0. The DLS experiments were conducted as a function of increasing citric acid concentration with a suspension concentration of 0.01 g/L TiO<sub>2</sub>. At pH 2.0, nanoparticle aggregate size increases with added citric acid. At pH 6.0, nanoparticle aggregate size decreases with added citric acid.

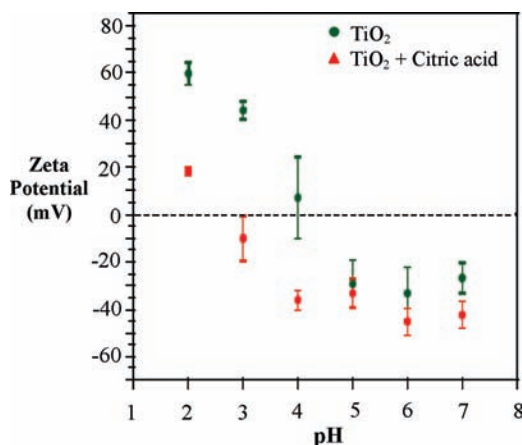


**Figure 7.** Zeta potential measurements of TiO<sub>2</sub> (0.05 g/L) in the absence (green) and the presence (red) of citric acid (0.1 mM) as a function of pH.

the sedimentation data presented in Figure 5. The DLS data collected at nanoparticle suspensions of 0.01 g/L clearly show that at pH 2.0 aggregate size increases with increasing concentration, whereas at pH 6.0, aggregate size decreases with increasing concentration of citric acid.

Taking the adsorbed speciation and the mode of adsorption suggested by the spectroscopic data, the reversal of the suspension stabilities can be attributed to the surface charge modification by the adsorbed citrate.<sup>14,16,23</sup> Adsorbed citrate is a trianion (Figure 3) and TiO<sub>2</sub> surface is positively charged at pH 2.0. The adsorption of the citrate neutralizes the surface charge to a greater extent and thereby reduce the double layer formation leading to the observed enhanced aggregation at pH 2.0. At pH 6.0, the adsorbed citrate could have created a negative charge on the neutral surface leading to a double layer formation thereby increasing the repulsive forces (charge stabilization).

Zeta potential measurements support the data shown in Figures 5 and 6. In general, zeta potentials measure the net charge at the diffuse boundary of a particle. It is generally assumed that zeta potentials close to zero result in unstable suspension and nanoparticle aggregation. Figure 7 shows differences in the zeta potential for TiO<sub>2</sub> in the presence and absence of citric acid. These data show that at pH 2.0 citric

acid shifts the zeta potential for TiO<sub>2</sub> nanoparticle suspensions toward zero (from +60 to +19 mV) and thus decreases the nanoparticle suspension stability as confirmed by the sedimentation plots and DLS aggregate size measurements. However, at pH 6.0, citric acid shifts the zeta potential measurement for TiO<sub>2</sub> nanoparticle suspensions further away from zero (from −33 to −45 mV). Thus, it is clear that the presence of citric acid affects the surface charge under pH conditions and the direction of change supports the molecular measurements that show surface charge alterations upon adsorption; That is, the deprotonated citric acid on the surface lowers the net surface charge toward zero at acidic pH conditions and increases the net negative charge at circumneutral pH conditions. The shift in the surface charge (although not very large) seems to be enough to overcome the activation barrier for aggregation at pH 2.0 while increase the energy barrier for aggregation at pH 6.0. These observations and hypotheses are supported using DLVO theory along with measured zeta potential values at the different pH conditions. According to DLVO, nanoparticle–nanoparticle interactions are determined by the potential energy between two nanoparticles which is a sum of the attractive and repulsive interactions

$$V_{\text{tot}} = V_{\text{att}} + V_{\text{rep}} \quad (1)$$

due to van der Waals and electrostatic interactions, respectively. Attractive forces are a function of particle size and the Hamaker constant which accounts for interparticle interactions. Repulsive forces are due to surface charge and electrostatic interactions as measured by the zeta potential. According to these calculations, nanoparticle suspensions at pH 2.0 in the absence of citric acid are the most stable with the highest nanoparticle–nanoparticle repulsive barrier of nearly 3  $k_B T$ , whereas in the presence of citric acid, pH 6.0 suspensions are most stable and show the highest nanoparticle–nanoparticle repulsive barrier of 1.5  $k_B T$  (see Supplemental Figure 4).

Similar studies done on TiO<sub>2</sub> nanoparticles in the presence of oxalic acid and Suwannee River Fulvic Acid (SRFA) have shown different trends in aggregation.<sup>23,24</sup> According to Pettibone et al., the presence of oxalic acid at pH 2.0 has shown a similar enhanced aggregation but the aggregation at pH 6.5 had remained unaffected.<sup>24</sup> Analysis of the surface charge in the presence of oxalic acid showed that at pH 2.0 the surface charge is shifted from +25 to +4 mV which is a much similar to the case of citric acid. However, at pH 6.0, the surface charge has shifted from −33 to −23 mV with oxalic acid and the sedimentation behavior remained unaffected. The difference in the aggregation behavior at pH 6.0 for oxalic and citric acid could be a result of increased electrostatic and steric repulsions present in the citric acid–TiO<sub>2</sub> compared to oxalic acid–TiO<sub>2</sub>. DLVO theory suggests that the repulsive forces form an energy barrier for the particle aggregation. Only the particles that collide with sufficient energy to overcome this barrier will form aggregates. These repulsive forces can be steric and/or electrostatic. A study by Domingos et al. has shown decreased aggregation in the presence of SRFA from highly acidic medium up to pH 6.0 after which there is an increase in the aggregation.<sup>23</sup> SRFA has high steric repulsions resulting in a very high energy barrier for aggregation. Therefore, the observed decrease in aggregation for SRFA is to be expected. Domingos et al. suggest that the increase in the aggregation for higher pH conditions

(23) Domingos, R. F.; Tufenkji, N.; Wilkinson, K. J. *Environ. Sci. Technol.* **2009**, *43*, 8178–8183.

(24) Pettibone, J. M.; Cwiertny, D. M.; Scherer, M.; Grassian, V. H. *Langmuir* **2008**, *24*, 6659.

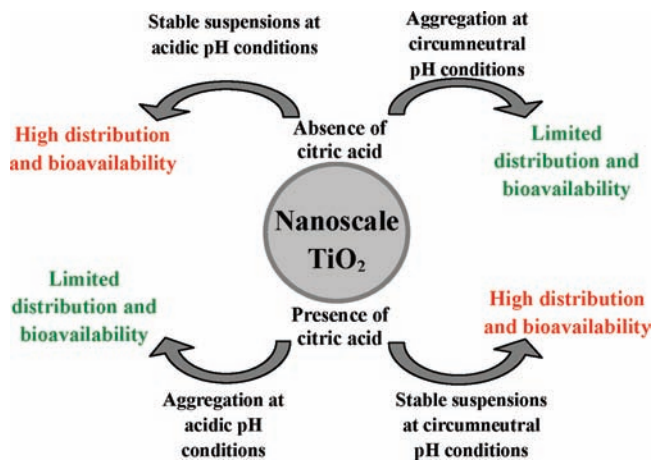


**Figure 8.** A summary of the behavior of nanoscale TiO<sub>2</sub> particles as a function of pH and citric acid at fixed ionic strength (0.03 M).

was due to a different mechanism involving bridging of nanoparticles by SRFA.

Because aggregation behavior can be altered upon co-adsorption of other species, sedimentation studies were also conducted in the presence of both citric acid (3 mM) and oxalic acid (3 mM) at pH 2.0 and 6.0 (see Supplemental Figure 5). These data show that the aggregation behavior of TiO<sub>2</sub>–citrate prevails even in the presence of oxalic acid and shows that TiO<sub>2</sub> has a greater affinity toward citric acid compared to oxalic acid.

Aggregation of nanoparticles is of great significance to its environmental fate and transport.<sup>23,25–27</sup> The larger aggregates are known to sediment out which will limit their distribution in the environment. Furthermore, recent studies have shown that the ability of nanoparticles to undergo dissolution can be quenched upon aggregation.<sup>28,29</sup> This study shows that at near circumneutral conditions citrate has an inhibiting effect on TiO<sub>2</sub> nanoparticle aggregation leading to potentially high distribution. As citrate is also abundant in human plasma, upon inhalation of these nanoparticles, there is a greater risk of them distributing throughout the body as well. The true extent of these implications is yet to be realized due to lack of quantitative data for nanoparticle levels in the environment and in vivo. Although the behavior of nanomaterials in the environment or in vivo remains uncertain due to the complex nature of the *milieu*, a summary of the results discussed here with respect to nanoparticle–nanoparticle interactions at different pH and the impact of a citric acid, a common ligand, is presented in Figure 8 as a guide to begin to understand this complexity as it relates to the distribution and bioavailability of nanoscale TiO<sub>2</sub>.

## Conclusions and Implications

A number of interesting and important conclusions come from the results of these studies of citric acid adsorption as a function of pH and its impact on nanoparticle–nanoparticle interactions. First, the adsorption of citric acid onto 4 nm TiO<sub>2</sub> nanoparticles is a pH dependent process with surface coverage decreasing as

a function of pH. Second, although citric acid solution speciation is highly pH dependent in the range investigated here (2.0–7.5), surface speciation was found to differ and after equilibration shown to be the completely deprotonated form at highly acidic solution pH, and at pH 2.0, surface adsorption changes from a partially deprotonated form to the fully deprotonated form over time scales of minutes to hours. Thus, surface adsorption increases the acidity of citric acid resulting in a loss of protonated carboxylate groups lower than expectations based on solution  $pK_a$  values. Third, the adsorption of citric acid is irreversible at  $T = 293$  K suggesting strong coordination to the surface which is indicative of an inner sphere complex to the surface with one or more carboxylic groups. Fourth, nanoparticle–nanoparticle interactions occur under all pH conditions considered but the degree of aggregation changes as a function of solution pH with the greatest degree of aggregation occurring around  $pH_{zpc}$  and the lowest in highly acidic pH. Fifth, the presence of citrate alters the aggregation behavior at both highly acidic and neutral pH conditions by altering the surface charge of the nanoparticles. At pH 2.0, this results in the destabilization of relatively stable suspensions in the presence of citrate with the formation of aggregates. In contrast, at pH 6.0, TiO<sub>2</sub> suspensions are unstable and large aggregates are present; however, in the presence of citrate, aggregation was hindered and suspensions were more stable. These trends observed in aggregation of TiO<sub>2</sub> nanoparticles in the presence of citrate are of environmental and biological significance as aggregation plays a key role in controlling the distribution of these particles in aquatic environments and cellular matrices as well as in the body where citric acid is found in abundance. Thus, the studies discussed here provide important insight into the behavior of some of the smallest TiO<sub>2</sub> particles and their surface chemistry with citric acid.

Furthermore, it is well-known that the development of nanomaterials for use in a wide range of fields including medicine, solar energy conversion, water purification, and catalysis is of great interest.<sup>25,26,30–34</sup> Among a large number of these engineered nanomaterials, nanoscale TiO<sub>2</sub> is of great interest due to some of its unique characteristics, including its high refractive index for use in plastics, enamels, artificial fibers, electronic material, and rubber. Its ability to absorb solar light makes it useful in solar panels. It is a self-cleaning disinfectant, an effective photocatalyst, and a good support material for heterogeneous catalysts.<sup>32</sup>

With increasing use, recent studies have in fact shown that TiO<sub>2</sub> is in the environment and indeed have found convincing evidence of its presence both in the atmosphere and hydrosphere. In some cases, there is evidence that it is from anthropogenic sources.<sup>33,34</sup> A study conducted by Kaegi et al. shows the emission of engineered TiO<sub>2</sub> nanoparticles from the exterior facades into natural water and the presence of these particles in the urban runoff.<sup>34</sup> Zheng et al. has detected Ti-rich inhalable particulates in the atmosphere.<sup>33</sup> An exposure model developed by Mueller et al. has suggested annual worldwide production of nanoscale TiO<sub>2</sub> as of 2008 is nearly 5000 tons, hence,

(25) Mueller, N. C.; Nowack, B. *Environ. Sci. Technol.* **2008**, *42*, 4447.

(26) Baun, A.; Hartmann, N. B.; Grieger, K. D.; Hansen, S. F. *J. Environ. Monit.* **2009**, *11*, 1774.

(27) French, R. A.; Jacobson, A. R.; Kim, B.; Isley, S. L.; Penn, R. L.; Baveye, P. C. *Environ. Sci. Technol.* **2009**, *43*, 1354.

(28) Liu, J.; Araguete, D. M.; Murayama, M.; Hochella, M. F. *Environ. Sci. Technol.* **2009**, *43*, 8178–8183.

(29) Rubasinghe, G.; Lentz, R. W.; Park, H.; Scherer, M. M.; Grassian, V. H. *Langmuir* **2009**, *26*, 1524.

(30) Sharma, V. K. *J. Environ. Sci. Health, Part A: Toxic/Hazard. Subst. Environ. Eng.* **2009**, *44*, 1485.

(31) Boncagni, N. T.; Otaegui, J. M.; Warner, E.; Curran, T.; Ren, J. H.; De Cortalezzi, M. M. F. *Environ. Sci. Technol.* **2009**, *43*, 7699.

(32) Hadjiivanov, K. I.; Klissurski, D. G. *Chem. Soc. Rev.* **1996**, *25*, 61.

(33) Zheng, N.; Wang, H. J. *Spectrosc. Spectral Anal.* **2009**, *29*, 1570.

(34) Kaegi, R.; Ulrich, A.; Sinnet, B.; Vonbank, R.; Wichser, A.; Zuleeg, S.; Simmler, H.; Brunner, S.; Vonmont, H.; Burkhardt, M.; Bollner, M. *Environ. Pollut.* **2008**, *156*, 233.



increasing the potential of this material getting into the environment.<sup>25</sup> The model simulation predicts  $1.5 \times 10^{-3} \mu\text{g m}^{-3}$ ,  $0.7 \mu\text{g L}^{-1}$ , and  $0.4 \mu\text{g kg}^{-1}$  of nanoscale  $\text{TiO}_2$  in air, water, and soil, respectively. Grassian et al. has shown that subacute exposure of 2–5 nm sized  $\text{TiO}_2$  nanoparticles results in moderate but statistically significant inflammatory responses among animals at weeks 0, 1, or 2 and resolves after 3 weeks.<sup>12</sup> Furthermore, the studies of Sun et al. on higher uptake of As(V) in aquatic animals in the presence of nanoscale  $\text{TiO}_2$  highlight the enhanced transport of known contaminants via co-transport.<sup>30</sup> Thus, understanding the behavior of nanomaterials especially in natural water systems is complex due to a number of factors including pH, ionic strength, and the presence of complexing molecules.<sup>23,24,35,36</sup> Furthermore, nanoparticle aggregation adds to the complexity and questions the validity of high concentration–toxicity relationships due to a potential decrease in bioavailability of the aggregated particles.<sup>26</sup> Investigations of the behavior of nanomaterials in these simpler

systems such as the ones discussed here offer some insights into their behavior in the more complex matrices found in nature.

**Acknowledgment.** The research described in this article has been funded wholly or in part by the Environmental Protection Agency through grant number EPA R83389101-0 to V.H.G. The authors would like to thank Dr. Shaowei Bian for help with DLVO calculations.

**Supporting Information Available:** Supplemental Figure 1 shows calibration data and linearity for sedimentation plots. Supplemental Figure 2 shows isotherms for the adsorption of citric acid as a function of pH. Supplemental Figure 3 shows additional ATR-FTIR spectra recorded for citric acid as a function of pH. These spectra show that at the concentrations used in the adsorption measurements, contributions from absorptions of solution phase species are minimal compared to adsorbate absorptions. Supplemental Figure 4 shows the aggregation behavior in the presence of both oxalic and citric acid. This material is available free of charge via the Internet at <http://pubs.acs.org>.

JA106091Q

(35) Ridley, M. K.; Hackley, V. A.; Machesky, M. L. *Langmuir* **2006**, *22*, 10972.

(36) Yang, K.; Lin, D. H.; Xing, B. S. *Langmuir* **2009**, *25*, 3571.